Analysis of $\pi^{\pm}$-nucleus elastic scattering using a local potential

S. A. E. Khallaf and A. A. Ebrahim
Physics Department, Faculty of Science, Assiut University, Assiut 71516, Egypt
(Received 7 September 1999; published 13 July 2000)

Pion-nucleus scattering has been analyzed using an equivalent local potential to calculate the differential cross sections for pions elastically scattered from ^{12}C, ^{16}O, ^{28}Si, and ^{40,44,48}Ca in the energy range of 30 to 292 MeV. The DWUCK4 computer program was used to predict observables of pion-nucleus elastic scattering. Our results are successfully compared to recent data. The skin neutrons in ^{44,48}Ca contribute to $\pi^{\pm}$ elastic scattering in this energy range more than the protons.

PACS number(s): 25.80.Dj, 24.10.−i

I. INTRODUCTION

Satchler [1] introduced a local, phenomenological optical potential of Woods-Saxon shape to describe—with great success—the angular distributions of the differential cross sections for elastic and inelastic scattering of positive and negative pions ($\pi^{\pm}$) from the nuclei ^{40,48}Ca, ^{58}Ni, ^{90}Zr, ^{118}Sn, and ^{208}Pb at energies ranging from 100 to 300 MeV. In his analysis, Satchler used the PTOLEMY computer code, which began as a program for heavy-ion direct-reaction calculations.

On the other hand, Johnson and Satchler [2] derived local potentials at both low and resonance energies equivalent to nonlocal Kisslinger-type potentials on the basis of multiple scattering theory. With these equivalent potentials, differential cross sections for (π^{+}) elastically scattered from ^{16}O at 162 MeV were calculated. The local potentials of ($\pi^{\pm}$) + ^{208}Pb at energies ranging from 20 to 291 MeV were also calculated.

It may be useful to mention here that two forms of potential are commonly used to describe the pion-nucleus interaction. These two forms are the Kisslinger [3] potential and a Laplacian [4] one. Both contain explicitly terms that originate in the *p*-wave pion-nucleon interaction important near the 3-3 resonance energy at 160 MeV. The Kisslinger potential [3] is

$$U_k(r)=\frac{(\hbar c)^2}{2\omega}\{q(r)+\nabla\cdot\alpha(r)\nabla\}, \tag{1.1}$$

where ω is the total energy of the pion in the center of mass (c.m.) system, $q(r)$ primarily results from the *s*-wave part, and $\alpha(r)$ results from the *p*-wave part of the pion-nucleon interaction, $q(r)$ and $\alpha(r)$ being expressed in terms of the nuclear densities of the target nucleus. Both are complex and energy dependent. In the Laplacian model the potential is local and is written as

$$U_L(r)=\frac{(\hbar c)^2}{2\omega}\left\{q(r)-k^2\alpha(r)-\frac{1}{2}\nabla^2\alpha(r)\right\}, \tag{1.2}$$

with $q(r)$ and $\alpha(r)$ the same as for the Kisslinger potential, and k the wave number of the pion-nucleon in the center of momentum frame. Since the Kisslinger potential satisfies all features of $\pi^{\pm}$-nucleus interactions, it has been suggested that the Kisslinger potential and not the Laplacian one is the more suitable for describing pion-nucleus interactions [5].

In the present work, the equivalent local potential of Johnson and Satchler [2] is used to analyze the elastic scattering of $\pi^{\pm}$ from ^{12}C, ^{16}O, ^{28}Si, and ^{40,44,48}Ca in the pion kinetic energy range of 30 to 292 MeV, where the local potentials are easier to visualize than the nonlocal versions. Two density distribution forms and only two Ericson-Ericson Lorentz-Lorentz parameter values are used.

The DWUCK4 code that solves the nonrelativistic Schrödinger equation is employed in the present analysis, since the DWUCK4 program is widely available. This program was originally written to calculate the scattering and reaction observables for binary nuclear reactions using the distorted-wave Born approximation [6]. Our results from calculating angular distributions of the differential cross sections for the elastic scattering of $\pi^{\pm}$ from the above mentioned nuclei are compared to the corresponding experimental data. As far as we know, this is the first use of the DWUCK4 computer code and the equivalent local potential to calculate the elastic scattering differential cross section angular distributions for pions.

II. FORMALISM

For the Kisslinger nonlocal potential, Johnson and Satchler [2] used the Krell-Ericson transformation, which leads from the Klein-Gordon equation for pion scattering to a local potential for the transformed wave function. Thus, a standard nonrelativistic optical model computer program may be used to calculate the angular distribution for a pion scattered from a nucleus. Such a program should be provided with an effective pion mass, the target mass, and an effective pion energy. The transformed wave function ψ satisfies a Schrödinger equation:

$$\{-(\hbar^2/2\mu)\nabla^2+U_L+V_C\}\psi=E_{\text{c.m.}}\psi. \tag{2.1}$$

To solve Eq. (2.1) for pion elastic scattering from a nucleus we employed the DWUCK4 computer code [6] with a reduced mass μ:

$$\mu=M_\pi m_T/(M_\pi+m_T), \tag{2.2}$$

where m_T is the target mass and the effective pion mass is $M_\pi=\gamma_\pi m_\pi$. γ_π is defined as [1]

$$\gamma_\pi = \frac{y+\gamma_l}{(1+y^2+2y\gamma_l)^{1/2}}, \quad y = m_\pi/m_T,$$
$$\gamma_l = 1+(K_l/m_\pi c^2), \tag{2.3}$$

where K_l is the pion bombarding energy in the laboratory system and m_π is the pion mass. Here $m_\pi c^2 = 139.6$ MeV has been used. The center-of-mass kinetic energy $E_{\text{c.m.}}$ is

$$E_{\text{c.m.}} = (\hbar k)^2/2\mu, \tag{2.4}$$

where $\hbar k$ is the center-of-mass momentum of the incident pion. The effective bombarding energy E_l [1] is

$$E_l = E_{\text{c.m.}}(M_\pi + m_T)/m_T, \tag{2.5}$$

which will generate the appropriate k value in the form

$$k = \left(\frac{m_\pi c}{\hbar}\right)(\gamma_\pi{}^2-1)^{1/2} = 4.720\,56 m_\pi(\gamma_\pi{}^2-1)^{1/2} \ \text{fm}^{-1}, \tag{2.6}$$

where $m_\pi = 0.1499$ atomic mass units (u). The kinematics parameters for the cases studied here are calculated using Eqs. (2.2)–(2.6).

In Eq. (2.1), V_C is the Coulomb potential due to the uniform charge distribution of the target nucleus of radius $R_C = r_C A^{1/3}$ and A is the target mass number. Here $r_C = 1.2$ fm is considered [1]. U_L is the nuclear local transformed potential and is given in detail in Ref. [2]. It is constructed from S-wave and P-wave pion-nucleon interaction parts. The P-wave part includes the Ericson-Ericson Lorentz-Lorentz (EELL) parameter ζ [2]. In this work, two values of the EELL parameter are considered, namely, $\zeta = 1.8$ [7] and $\zeta = 1.0$ [2], where we restricted ourselves to those two values of ζ used in Ref. [2]. We have found that this parameter is important to give good fits to data. Both S-wave and P-wave parts depend on pion-nucleon scattering amplitudes, the target density distribution, and its gradient. The pion-nucleon scattering amplitude depends on complex first-order and second-order interaction parameters. The first-order interaction parameters are related to the free pion-nucleon scattering through phase shifts in the form described in Ref. [8]. Here, the phase shifts δ_l are calculated according to the recent relation of Ref. [9]:

$$\frac{\tan\delta_l}{q^{2l+1}} = b + cq^2 + dq^4 + \frac{x\Gamma\omega_0 q_0^{-(2l+1)}}{\omega_0^2-\omega^2}, \tag{2.7}$$

where the resonance energy is ω_0, its width is Γ, the strength parameter $x = 2|r|/\Gamma, |r|$ is the absolute value of the residue for each pole, q_0 is the center-of-mass momentum of the π-N system to reach ω_0, and l is the angular momentum quantum number. This parametrization was used in Ref. [9] to compute the π-nucleus scattering with the nonlocal Kisslinger potential. The resonance parameters and coefficients b, c, and d are taken from Ref. [9]. The first-order parameters b_i and c_i $(i=0,1)$ for various pion kinetic energies T_π and targets considered here are calculated through Eq. (2.7).

Next, we present the results of studies of the sensitivity of the local potential and the associated differential cross sections to the choice of the model used for the density distribution; we use simple two-parameter and three-parameter Fermi shapes for the density distributions for the studied nuclei. Thus,

$$\rho(r) = \rho_n(r) + \rho_p(r). \tag{2.8}$$

The three-parameter Fermi (3PF) form is

$$\rho_i(r) = \rho_{0i}(1+\omega_i r^2/c_i{}^2)/\{1+\exp[(r-c_i)/a_i]\} \tag{2.9}$$

$(i = n$ for neutrons, p for protons). The two-parameter Fermi (2PF) form is easily obtained from the above expression for the 3PF form $\omega_i = 0.0$ and ρ_{0i} $(i=n,p)$ can be evaluated from the normalization condition

$$\int \rho_i(r)d\bar{r} = (A-Z) \ \text{or} \ Z, \tag{2.10}$$

which yields

$$\rho_{0i}(r) = \frac{(A-Z) \ \text{or} \ Z}{4\pi(I_1+\omega_i I_2)}, \tag{2.11}$$

where

$$\mathrm{I}_1 \simeq \frac{1}{3}[c_i^3 + (a_i\pi)^2 c_i],$$
$$\mathrm{I}_2 \simeq \frac{1}{5}c_i{}^3 + \frac{2}{3}(a_i\pi)^2 c_i + \frac{7}{15}\frac{(a_i\pi)^4}{c_i},$$

and Z is the atomic number of the nucleus. The parameters c_i, a_i, and w_i $(i=n,p)$ are given in Table I [2,10–13].

The root mean square radii for nuclei considered here are calculated and the results of our calculations are included in Table II compared to those from Ref. [14].

III. DISCUSSION

Using the interaction parameters for calculating the nuclear potential of elastic scattering of $\pi^\pm$ from ^{12}C, ^{16}O, ^{28}Si, and ^{40,44,48}Ca and inserting this potential U_L added to V_C into the DWUCK4 code, the results obtained for angular distributions of differential elastic cross section are shown in Figs. 1–6. The first-order parameters b_i and c_i $(i=0,1)$ are calculated through the phase shift equation (2.7), as they are computed in the code of Ref. [9]. These parameters b_i and c_i are then used to generate the complex local potential U_L using the expressions from Ref. [2]. The same coefficients b_i and c_i are also used for calculations in the

TABLE I. Ground-state density distribution parameters for the three- and two-parameter Fermi functions. n is for neutrons and p for protons.

Nucleus	Model	c_p (fm)	a_p (fm)	w_p	c_n (fm)	a_n (fm)	w_n	Reference
^{12}C	3PF	2.002	0.383	0.540	2.002	0.383	0.540	[10]
	2PF	2.5	0.37	0.0	2.5	0.37	0.0	[11]
^{16}O	3PF	2.608	0.513	−0.051	2.608	0.513	−0.051	[12]
	2PF	2.60	0.45	0.0	2.60	0.45	0.0	[2]
^{28}Si	3PF	3.34	0.58	−0.233	3.34	0.58	−0.233	[10]
	2PF	3.14	0.537	0.0	3.14	0.537	0.0	[10]
^{40}Ca	3PF	3.68	0.546	−0.1	3.97	0.42	−0.1	[13]
	2PF	3.42	0.55	0.0	3.42	0.55	0.0	[13]
^{44}Ca	3PF	3.750	0.530	−0.09	4.060	0.470	−0.09	[13]
	2PF	3.55	0.55	0.0	3.52	0.55	0.0	[13]
^{48}Ca	3PF	3.74	0.48	−0.03	4.06	0.46	−0.03	[13]
	2PF	3.47	0.55	0.0	3.63	0.55	0.0	[13]

Kisslinger model to compare to the local potential calculations.

Examples are taken for a wide range of energies from 30 MeV to 292 MeV. We found that there are two factors that play a significant role in our calculations in order to have a good fit with the data. First is the form of the density distributions. We used the two parameter Fermi as well as the three- parameter Fermi forms. Second, the EELL parameter ζ is found to play a significant role in the calculations. The positions of the minima seen in the data are reproduced by our calculations with $\zeta=1.0$, while these minima are found to move toward forward angles with the value $\zeta=1.8$.

In the figures we use solid curves for the 3PF and $\zeta=1.0$, thick solid curves for the 2PF and $\zeta=1.0$, dot-dashed curves for the 3PF and $\zeta=1.8$, dotted curves for the 2PF and $\zeta=1.8$ results of the present work, and dashed curves for the previous calculations using the first-order distorted wave impulse approximation code DWPI [9].

π^--^{12}C differential elastic cross sections have been calculated at two energies 120 and 280 MeV, where the local optical potential was computed by our modified DWUCK4 code. The comparsions between our calculations and the experimental data of Binon *et al.* [15] are represented in Fig. 1. We have excellent agreement between the theoretical calculations and data when we use the 3PF distribution and $\zeta=1.0$. Figure 1 shows that the EELL parameter has a large effect; the value of $\zeta=1.8$ destroys the agreement with the π^--^{12}C elastic scattering data. A significant difference between the experimental data and the present computations for π^--^{12}C elastic scattering is found when we use the 2PF distribution. Also, $\zeta=1.8$ moves the minima toward the forward angles. There are no differences between the present local potential calculations with 3PF and $\zeta=1.0$ and those based on DWPI [9].

Figure 2 shows the differential elastic cross sections of π^+ from ^{16}O at 114 MeV. Data [16] are compared to DWPI and the present local potential calculations. The present local potential calculations using the 3PF distribution and $\zeta=1.0$ and DWPI calculations are almost indistinguishable and agree well with the data [16], while the calculations based on the present local potentials are far from the data when $\zeta=1.8$. The local potential gives poor agreement with the experi-

TABLE II. rms radii in fm for the density distributions used in the present calculations.

		This calculation			Estimated by others [14]
Nucleus	Model	$\langle r^2\rangle_p^{1/2}$	$\langle r^2\rangle_n^{1/2}$	$\langle r^2\rangle_m^{1/2}$	$\langle r^2\rangle_m^{1/2}$
^{12}C	3PF	2.32324	2.32324	2.32324	2.314
	2PF	2.37521	2.37521	2.37521	
^{16}O	3PF	2.72657	2.72657	2.72657	2.596
	2PF	2.61802	2.61802	2.61802	
^{28}Si	3PF	3.07564	3.07564	3.07564	3.001
	2PF	3.14647	3.14647	3.14647	
^{40}Ca	3PF	3.40659	3.39968	3.38278	3.366
	2PF	3.34628	3.34628	3.34628	
^{44}Ca	3PF	3.44257	3.54624	3.49973	3.410
	2PF	3.42655	3.40793	3.41629	
^{48}Ca	3PF	3.38469	3.56398	3.56304	3.566
	2PF	3.37703	3.47648	3.43210	

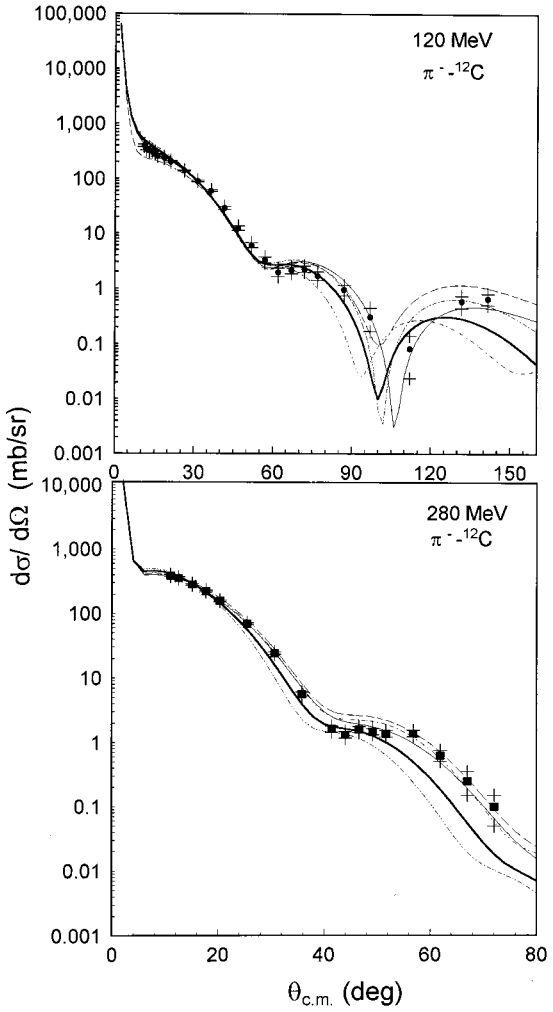

FIG. 1. π^--^{12}C differential elastic scattering cross sections at energies 120 and 280 MeV. The solid curves use the 3PF distribution and $\zeta=1.0$, thick solid curves use the 2PF and $\zeta=1.0$, dot-dashed curves use the 3PF and $\zeta=1.8$, while dotted curves use the 2PF and $\zeta=1.8$ of the present work, and dashed curves use the new phase shift calculations from DWPI [9]. Solid points are the experimental data taken from Ref. [15].

mental data [16] on using the 2PF density distribution with both values of $\zeta=1.0$ and 1.8.

In Figs. 3 we show the differential elastic scattering cross sections of $\pi^{\pm}$-^{28}Si at 130 MeV [17]. The two computations, DWPI and the present local potentials with the 3PF form and $\zeta=1.0$, give good agreement with the elastic scattering data [17]. Also shown in Figs. 3 are the calculated differential cross sections using $\zeta=1.8$ with the 3PF distribution; the fit is fairly good. On using the 2PF model with both values of $\zeta=1.0$ and 1.8, the calculations give poor agreement with data in these two cases.

We show in Figs. 4 and 5 elastic cross sections for π^+ at 180 MeV and π^- at 292 MeV on ^{40,44,48}Ca. Parameters for the density distributions of the nucleons in ^{40,44,48}Ca are taken to be those of Table I. Differential elastic cross sections computed with the present local potential using the 3PF distribution with $\zeta=1.0$ and DWPI based on the phase shifts

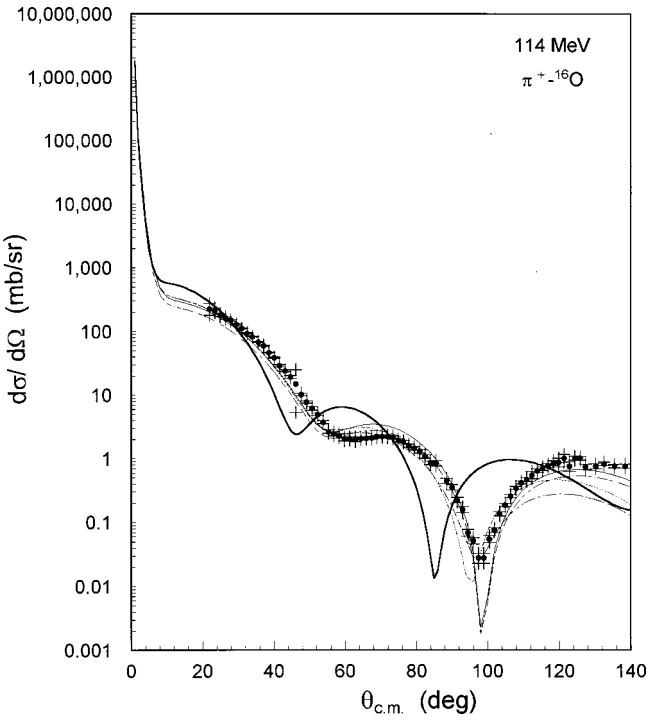

FIG. 2. As in Fig. 1 but for π^+-^{16}O differential elastic scattering cross sections. The experimental data are taken from Ref. [16] at energies of 114 MeV.

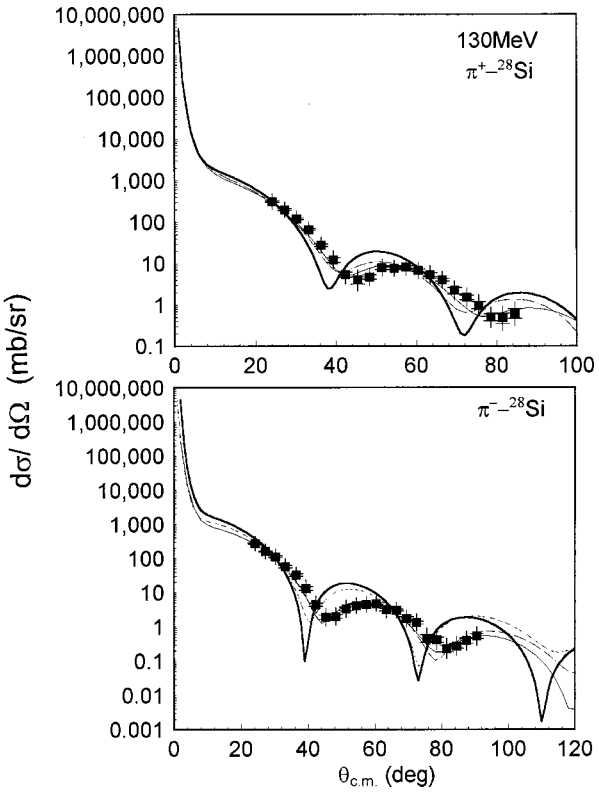

FIG. 3. As in Fig. 1 but for $\pi^{\pm}$-^{28}Si differential elastic scattering cross sections. The experimental data are taken from Ref. [17] at 130 MeV.

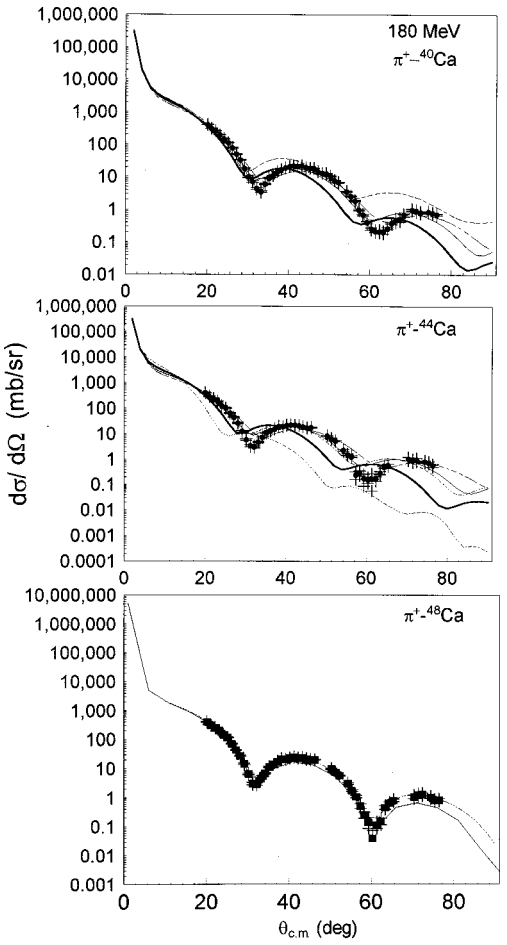

FIG. 4. As in Fig. 1 but for π^+-^{40,44,48}Ca differential elastic scattering cross sections at 180 MeV. The experimental data are taken from Ref. [13].

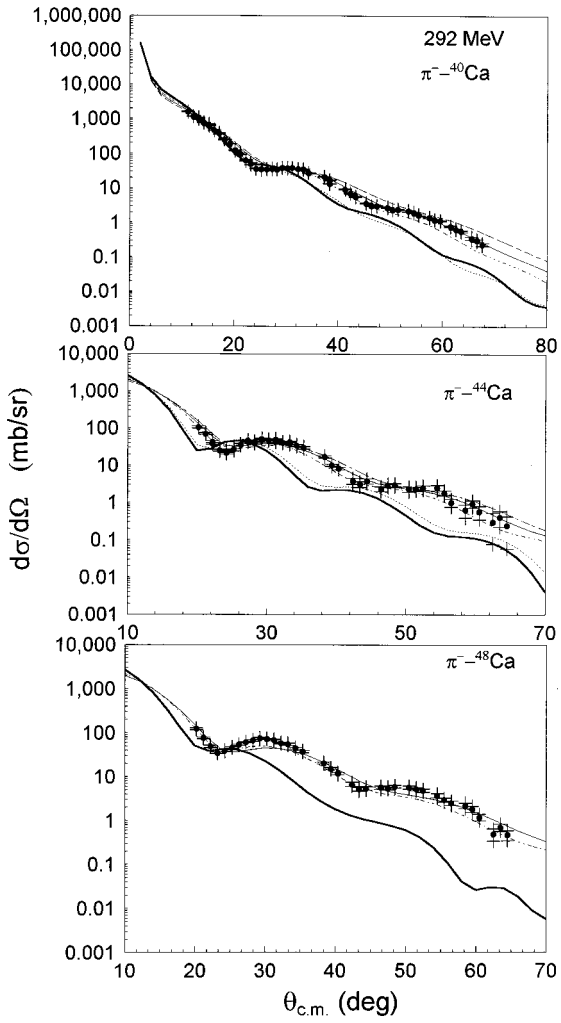

FIG. 5. As in Fig. 1 but for π^--^{40,44,48}Ca differential elastic scattering cross sections at 292.5 MeV. The experimental data are taken from Ref. [13].

[9] are identical and are in good agreement with the experimental data of Boyer *et al.* [13]. The EELL parameter $\zeta = 1.8$ moves the minima toward the forward angles in all cases considered. Also shown in Figs. 4 and 5 are the differential elastic cross sections for ^{40,44,48}Ca$(\pi^{\pm},\pi^{\pm})^{40,44,48}$Ca using the 2PF shape for the nucleons with both values of $\zeta = 1.0$ and 1.8. These computations are far from adequate, although the 2PF with $\zeta = 1.0$ gives reasonable agreement with data for some cases of $\pi^{\pm}$-^{40}Ca scattering at 180 and 292 MeV.

Moreover, elastic scattering differential cross sections for π^--^{12}C at 150, 180, and 200 MeV, π^+-^{16}O at 163 and 240 MeV, $\pi^{\pm}$-^{28}Si at 180 and 226 MeV, and $\pi^{\pm}$-^{40,44}Ca at 116 MeV are also calculated with the present local potential model where the experimental data are available [13,15–17]. In all cases considered, it is noted that the 3PF shape of the considered nuclei with the EELL parameter $\zeta = 1.0$ yields better fits to the experimental data than any other computations using 3PF with $\zeta = 1.8$ or the 2PF shape with $\zeta = 1.0$ or $\zeta = 1.8$.

At lower pion beam energies $T_\pi \leqslant 80$ MeV, the differential elastic cross sections for scattering of π^+ from ^{16}O and ^{40}Ca at energies of 30 and 50 MeV are calculated and compared to the experimental data [11]. Following Ref. [2] we have taken the complex second parameters B_1 and $C_1 = 0$. We compare in Fig. 6 the differential elastic cross sections for scattering of π^+ from ^{16}O at 30 MeV. Calculations in our modified first-order local optical potentials, using the 3PF with both values of $\zeta = 1.0$ and 1.8, have been done and compared with those from DWPI of Ref. [9]. Both calculations are unlike the data [11], especially at forward angles. When the second-order parameters B_0 and C_0 (see Ref. [2]) are included in addition to the first-order parameters b_0, b_1, c_0, and c_1 with both the present local potential and the DWPI code of Ref. [9] to compute the second-order curves in Fig. 6(a) we get good agreement with the data. These second-order parameters at 30 MeV are taken from Ref. [18]. The values are $B_0 = -0.162 + i0.103$ fm^4 and $C_0 = 0.747 + i0.615$ fm^6 at 30 MeV, while at 50 MeV they are $B_0 = 0.064 - i0.077$ fm^4 and $C_0 = 0.666 + i1.219$ fm^6. It is evident that the second-order parameters are very important at lower pion energies $T_\pi \leqslant 80$ MeV. For optical potentials

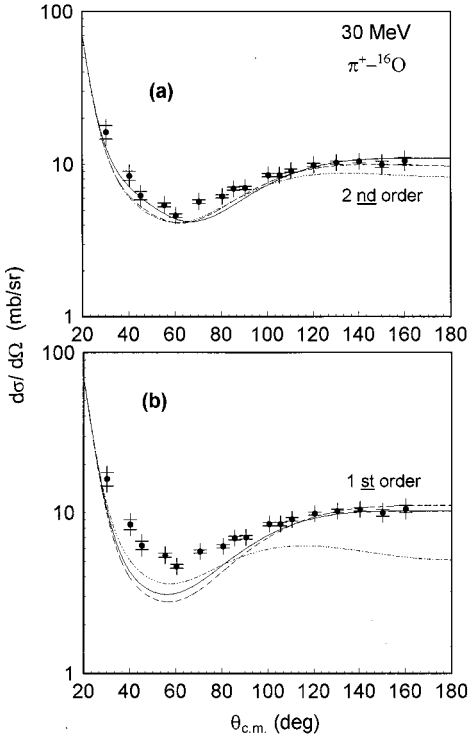

FIG. 6. (a) Differential elastic scattering cross sections of π^+ from ^{16}O at 30 MeV. The solid curves are for second-order local potential calculations using the 3PF form and $\zeta=1.0$, while dot-dashed curves use the 3PF and $\zeta=1.8$. The dashed curves use the second-order terms of [9]. Solid points are the experimental data taken from Ref. [11]. (b) The data [11] compared to first-order local potential calculations using the 3PF and $\zeta=1.0$ as the solid curves, the 3PF and $\zeta=1.8$ as the dot-dashed curves. The dashed curves use the first-order phase shifts calculations from DWPI [9].

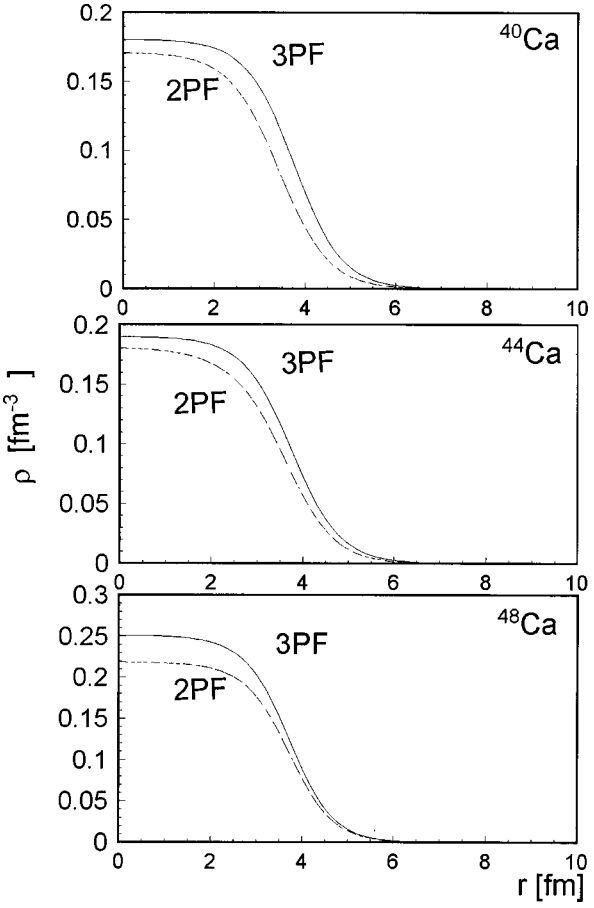

FIG. 7. The density distributions obtained from three-parameter Fermi and two-parameter Fermi shapes for Ca isotopes with parameters given in Table I.

these terms may take the form of higher powers in the density expansion (the so-called ρ^2 terms) [2].

The calcium isotopes have special significance in the study of nuclear radii because ^{40}Ca is often used for ''calibration'' of the projectile-target effective interaction and also because these isotopes span a wide range of neutron numbers, including two doubly closed shell nuclei ^{40,48}Ca, which are of particular interest for nuclear structure calculations. The root mean square (rms) radii are calculated for protons $\langle r^2\rangle_p^{1/2}$, for neutrons $\langle r^2\rangle_n^{1/2}$, and for nuclear matter $\langle r^2\rangle_m^{1/2}$ for all nuclei under consideration. These results are listed in Table II as well as $\langle r^2\rangle_m^{1/2}$ estimated by others [14]. The $\langle r^2\rangle_m^{1/2}$ calculated in the present work are very close to those estimated corresponding values except for ^{16}O.

In Table III, the differences between $\langle r^2\rangle_n^{1/2}$ and $\langle r^2\rangle_p^{1/2}$ are calculated for Ca isotopes and compared to the corresponding experimental values predicted from pion-calcium scattering at 180 MeV [13]. Also shown are the differences between $\langle r_m^2(A)\rangle^{1/2}$ and $\langle r_m^2(40)\rangle^{1/2}$ (in fm) extracted from Table II and compared to those of Ref. [19], where $A=44$ or 48. As can be seen from Table III, these differences deduced from the present work agree well with those of others except for the magnitude of $\langle r^2\rangle_n^{1/2}-\langle r^2\rangle_p^{1/2}$ for ^{40}Ca.

Figure 7 presents the density distributions obtained from 3PF and 2PF shapes for Ca isotopes. This figure indicates

TABLE III. From Table II in the case of 3PF, neutron minus proton rms radii for Ca isotopes compared with the corresponding values of Ref. [13], and nuclear matter rms radii for ^{44,48}Ca minus that of ^{40}Ca compared with the corresponding values of [19]. Values in fm.

Nucleus	$\langle r^2\rangle_n^{1/2}-\langle r^2\rangle_p^{1/2}$		$\langle r_m^2(A)\rangle^{1/2}-\langle r_m^2(40)\rangle^{1/2}$	
	Present calculation	From Ref. [13]	Present calculation	From Ref. [19]
^{40}Ca	-0.00691	-0.02 ± 0.04		
^{44}Ca	0.10367	0.11 ± 0.04	0.11695	0.10 ± 0.03
^{48}Ca	0.17929	0.18 ± 0.04	0.18026	0.18 ± 0.04

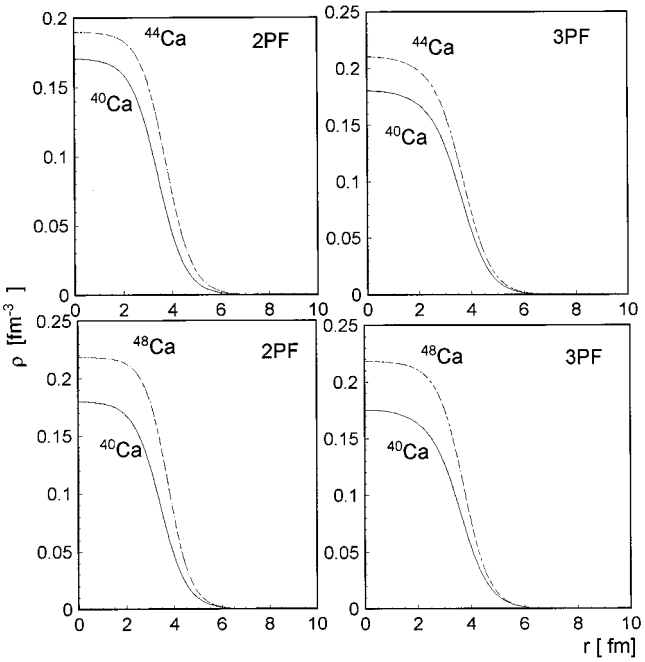

FIG. 8. Differences between the density distributions of ^{44,48}Ca and ^{40}Ca using the two forms of density shapes 2PF (left) and 3PF (right).

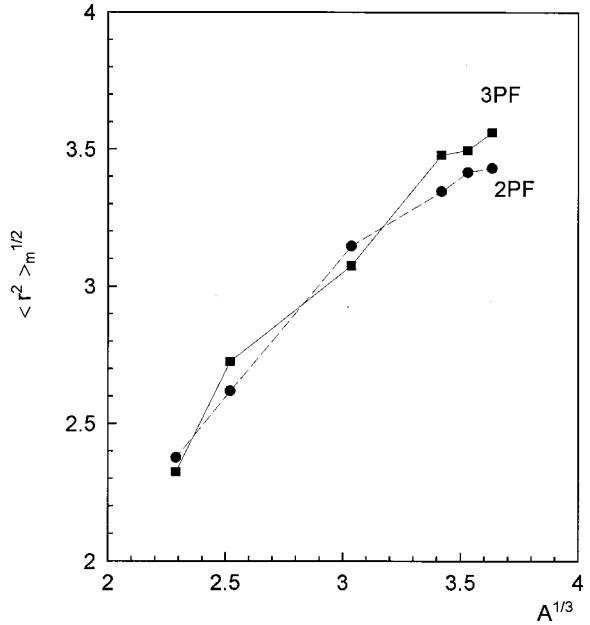

FIG. 9. The calculated rms radii of nuclear matter density distributions $\langle r^2\rangle_m^{1/2}$ using 3PF and 2PF against $A^{1/3}$ are shown. The solid and dashed lines are to guide the eye.

that the 3PF density distribution is higher than the 2PF in the central and surface regions for all Ca isotopes under consideration. This may be the reason that the 3PF distribution produces better agreement with the experimental data than the 2PF distribution, especially at backward scattering angles. But, as mentioned in Ref. [20], pions of $T_\pi \sim 20$–250 MeV can be completely absorbed in the surface region. It is also stated in Ref. [2] that the scattering in the resonance region is mostly sensitive to the potential in the surface. This means that the central density slightly affects the elastic scattering of $\pi^{\pm}$ differential cross sections. Therefore, it may be suggested that the distribution in the surface region is significant to predict well the elastic scattering differential cross sections at larger scattering angles.

Differences between the density distributions of ^{44,48}Ca and ^{40}Ca using the two forms of density shapes 2PF and 3PF are displayed in Fig. 8. These differences of the density shapes of the Ca isotopes show evidence for a neutron skin in ^{44,48}Ca. For convenience the calculated rms radii of nuclear matter density distributions $\langle r^2\rangle_m^{1/2}$ using 3PF and 2PF shapes against $A^{1/3}$ are shown in Fig. 9. This figure suggests that $\langle r^2\rangle_m^{1/2}$ increases linearly as $A^{1/3}$ increases. Table II also shows that the rms matter radii of the Ca isotopes increase with mass number. A considerable difference between proton and total matter distribution radii occurs for ^{48}Ca, indicating again a neutron skin for this nucleus. Therefore, it might be expected that the surface neutrons in ^{44,48}Ca have a larger effect than surface protons on fits with the $\pi^{\pm}$ elastic scattering experimental data up to about 300 MeV pion kinetic energy, while the central nucleons slightly affect the fitting.

IV. CONCLUSION

The conclusion reached from these calculations is that the local potential, without free parameters, gives a good description for the $\pi^{\pm}$-nucleus elastic scattering, especially if we limit ourselves to energies where the (3,3) resonance is dominant; the mean free path of the pion in the nuclear matter becomes small (~ 0.5 fm) [20], with the consequence that the interaction of the pion with the nucleus dominates in the nuclear surface. Also, we observe that the 3PF shape of the nuclear distributions along with the EELL parameter $\zeta = 1.0$ are more suitable for $\pi^{\pm}$ elastic scattering using the equivalent potential. The first-order local potential is adequate to give a good description of $\pi^{\pm}$-nucleus scattering at $T_\pi > 80$ MeV, whereas the second-order terms are required at lower energies $T_\pi \leqslant 80$ MeV. The skin neutrons in ^{44,48}Ca contribute to $\pi^{\pm}$ elastic scattering in this energy range more than protons. The rms radius for the nuclei considered increases linearly as $A^{1/3}$ increases.

Finally, it may be suggested that this work can be extended to use the DWUCK4 program to compute the $\pi^{\pm}$ inelastic scattering cross sections from nuclei. The success of this analysis with the DWUCK4 program may also set one up to compute the $\pi^{\pm}$ coupled channel reactions.

ACKNOWLEDGMENT

We would like to thank Professor R. J. Peterson, University of Colorado at Boulder, for a careful reading of the manuscript and for providing us with second-order parameters.

[1] G. R. Satchler, Nucl. Phys. **A540**, 533 (1992).
[2] M. B. Johnson and G. R. Satchler, Ann. Phys. (N.Y.) **248**, 134 (1996).
[3] L. S. Kisslinger, Phys. Rev. **98**, 761 (1955).
[4] G. Fäldt, Phys. Rev. C **5**, 400 (1972).
[5] E. Friedman, Phys. Rev. C **28**, 1264 (1983).
[6] P. D. Kunz, computer code DWUCK4, University of Colorado; P. D. Kunz and E. Rost, in *Nuclear Reactions*, Vol. 2 of *Computational Nuclear Physics*, edited by K. Langanke, J. A. Maruhn, and S. E. Koonin (Springer-Verlag, New York, 1993).
[7] O. Meivan, E. Friedman, R. R. Johnson, R. Olszewski, and P. Weber, Phys. Rev. C **40**, 843 (1989), and references therein.
[8] J. Bartel, M. B. Johnson, and M. K. Singham, Ann. Phys. (N.Y.) **196**, 89 (1989); S. J. Greene *et al.*, Phys. Rev. C **30**, 2003 (1984); R. A. Gilman, Ph.D. dissertation, University of Pennsylvania, 1985.
[9] A. A. Ebrahim and R. J. Peterson, Phys. Rev. C **54**, 2499 (1996).
[10] R. Alvarez del Castillo and N. B. de Takacsy, Phys. Rev. C **43**, 1389 (1991).
[11] B. M. Preedom *et al.*, Phys. Rev. C **23**, 1134 (1981).
[12] H. De. Vries *et al.*, At. Data Nucl. Data Tables **36**, 500 (1987).
[13] K. G. Boyer *et al.*, Phys. Rev. C **29**, 182 (1984).
[14] G. R. Satchler and W. G. Love, Phys. Rep. **55**, 183 (1979).
[15] F. Binon, P. Duteil, J. P. Garron, J. Gorres, L. Hugon, J. P. Peigneux, C. Schmit, M. Spighel, and J. P. Stroot, Nucl. Phys. **B17**, 168 (1970).
[16] J. P. Albanese, J. Arvieux, J. Bolger, E. Boschitz, C. H. Q. Ingram, J. Jansen, and J. Zichy, Nucl. Phys. **A350**, 301 (1980).
[17] B. M. Preedom, R. Corfu, J. P. Egger, P. Gretillat, C. Lunke, J. Piffaretti, J. Jansen, and C. Perrin, Nucl. Phys. **A326**, 385 (1979).
[18] R. J. Peterson (private communication).
[19] H. J. Gils, E. Friedman, Z. Majka, and H. Rebel, Phys. Rev. C **21**, 1245 (1980).
[20] S. A. Dytman *et al.*, Phys. Rev. C **19**, 971 (1979).